Author Manuscript

Author Manuscript

Author Manuscript

Author Manuscript

HHS Public Access

Author manuscript

*Curr Radiopharm*. Author manuscript; available in PMC 2022 January 01.

Published in final edited form as:

*Curr Radiopharm*. 2021 ; 14(1): 23–36. doi:10.2174/2211556009666200413085800.

# Thymoquinone Glucuronide Conjugated Magnetic Nanoparticle for Bimodal Imaging and Treatment of Cancer as a Novel Theranostic Platform

**İskender İnce**[1,2,*], **Zümrüt Biber Müftüler**[1], **E.İlker Medine**[1], **Özge Kozguş Güldü**[1], **Gökhan Takan**[1], **Ayşegül Ergönül**[3], **Yasemin Parlak**[5], **Yeliz Yıldırım**[2,4], **Burcu Çakar**[7], **Elvan Sayit Bilgin**[5], **Ömer Aras**[6], **Erdem Göker**[7], **Perihan Ünak**[*,1]

[1]Ege University, Department of Nuclear Application, Institute of Nuclear Sciences, Izmir, Turkey

[2]Ege University, Center for Drug R&D and Pharmacokinetic Applications (ARGEFAR), Izmir, Turkey

[3]Ege University, Faculty of Medicine Department of Chest Surgery, Izmir, Turkey

[4]Ege University, Faculty of Science, Department of Chemistry, Izmir, Turkey

[5]Celal Bayar University, Faculty of Medicine Department of Nuclear Medicine, Manisa, Turkey

[6]Memorial Sloan Kettering Cancer Center, Department of Radiology, New York, USA

[7]Ege University Faculty of Medicine, Division of Medical Oncology, Izmir, Turkey

## Abstract

**Background:** Theranostic oncology combines therapy and diagnosis and is a new field of medicine that specifically targets the disease by using targeted molecules to destroy the cancerous cells without damaging the surrounding healthy tissues.

**Objective:** We aimed to develop a tool that exploits enzymatic TQ release from glucuronide (G) for the imaging and treatment of lung cancer. We added magnetic nanoparticles (MNP) to enable magnetic hyperthermia and MRI, as well as 131**I** to enable SPECT imaging and radionuclide therapy.

**Methods:** A glucuronide derivative of thymoquinone (TQG) was enzymatically synthesized and conjugated with the synthesized MNP and then radioiodinated with 131**I**. New Zealand white

[*]Address correspondence to these authors at the Department of Nuclear Applications, Institute of Nuclear Sciences, Ege University, Bornova, P.O. Box: 35040, Izmir, Turkey; Tel/Fax: +90-232-388-6466; iskender.ince@ege.edu.tr; perihan.unak@gmail.com.

ETHICS APPROVAL AND CONSENT TO PARTICIPATE

This study was approved by the Animal Ethics Committee Ege University, Izmir Turkey (2014-021) and Celal Bayar University Animal Ethics Committee, Manisa, Turkey (2013-58).

HUMAN AND ANIMAL RIGHTS

No humans were involved in this study. All animal research procedures were performed in accordance with the standards of Guide for the US National Research Council's and Guide for the Care and Use of Laboratory Animals.

AVAILABILITY OF DATA AND MATERIALS

The datasets generated and/or analysed during the current study are not publicly available due to patented under Turkish Patent No TR 2015 10522 B but are available from the corresponding author [II] on reasonable request.

CONFLICT OF INTEREST

The authors declare no conflict of interest, financial or otherwise.

Author Manuscript Author Manuscript Author Manuscript Author Manuscript

rabbits were used in SPECT and MRI studies, while tumor modeling studies were performed on 6–7-week-old nude mice utilized with bioluminescence imaging.

**Results:** Fourier-transform infrared spectroscopy (FTIR) and nuclear magnetic resonance (NMR) spectra confirmed the expected structures of TQG. The dimensions of nanoparticles were below 10 nm and they had rather polyhedral shapes. Nanoparticles were radioiodinated with 131**I** with over 95% yield. In imaging studies, in xenograft models, tumor volume was significantly reduced in TQGMNP-treated mice but not in non-treated mice. Among mice treated intravenously with TQGMNP, xenograft tumor models disappeared after 10 and 15 days, respectively.

**Conclusion:** Our findings suggest that TQGMNP in solid, semi-solid and liquid formulations can be developed using different radiolabeling nuclides for applications in multimodality imaging (SPECT and MRI). By altering the characteristics of radionuclides, TQGMNP may ultimately be used not only for diagnosis but also for the treatment of various cancers as an *in vitro* diagnostic kit for the diagnosis of beta glucuronidase-rich cancers.

### Keywords

Thymoquinone; thymoquinone glucuronide; magnetic nanoparticles; lung cancer; iodine-131; SPECT; MRI; theranostics

## 1. INTRODUCTION

Lung cancer is the second most common cancer worldwide. Cancer formation in the lung is not the result of a sudden transforming event in the bronchial epithelium but a multistep process [1]. Although new treatment options, including immunotherapy, may prolong survival in lung cancer patients with advanced disease, there is still a lack of knowledge regarding how to identify patients in the early phase of cancer before it reaches a size that is detectable with standard radiologic techniques.

Using radionuclide-labeled active compounds for the early detection of lung cancer is very promising, yet it remains challenging even with advances to date in both nuclear imaging techniques and biotechnology. Chemotherapeutic agents used in the treatment of lung cancer are only available as intravenous formulations. Some of the leading chemotherapeutics are in lipophilic form and require higher doses to administer and/or solubilizing additives to improve drug delivery to tumor tissue. In addition, the oral administration of some chemotherapeutics is often limited due to first-pass metabolism [2, 3].

Theranostic oncology combines therapy and diagnosis and is a new field of medicine that specifically targets the disease by using targeted molecules to destroy the cancerous cells without damaging the surrounding healthy tissues [4]. Magnetic nanoparticles combining MRI contrast properties and magnetic hyperthermia properties have shown high theranostic potential; additionally, these nanoparticles have shown low toxicity, chemical stability, and non-carcinogenic properties [5-9]. Further more, magnetic nanoparticles can be combined with drug molecules, which can be guided to cancer cells in the body. Magnetic nanoparticles can exhibit PET/SPECT imaging properties when labelled with the proper radionuclides. Radionuclide-labeled tumor-targeting magnetic particles have been prepared in several studies: so far, $^{125}$I, $^{131}$I, $^{111}$In, $^{18}$F, $^{177}$Lu, and $^{89}$Zr-labeled magnetic

Author Manuscript Author Manuscript Author Manuscript Author Manuscript

nanoparticles have been introduced for PET/SPECT and MR imaging and/or therapy by several groups [5, 10-17].

According to the literature, lung cancer is known to be rich in the beta-glucuronidase enzyme [18, 19]. Su *et al.* showed that endogenous beta-glucuronidase activity can be visualized *in vivo* using micro-PET with a $^{124}$I-tyramine-conjugated difluoromethylphenol beta-glucuronide probe (TrapG). In their study, micro-PET and whole-body autoradiography showed that $^{124}$I-TrapG signals were 141.4 times higher in CT26/mbG tumors than in CT26 tumors [20].

For thousands of years, people have used natural products for the treatment of different diseases, despite the lack of efficacy, safety, and scientific validation. The traditional use of natural products has influenced medicine over the centuries. Nowadays, plants are considered as important sources in the development of new therapeutic agents for cancer, in addition to their traditional use in the treatment of various diseases. The development of spectral techniques has provided opportunities for elucidating the structures of secondary compounds found in plants and for investigating their bioactivity. As a result, many pharmaceutical products of plant origin have been introduced to support treatment, *e.g.*, paclitaxel (Taxol), one of the commonly used chemotherapy drugs, is obtained from *Taxus brevifolia* (Pacific yew) [21].

Thymoquinone is a phytochemical compound that has shown to be effective for the treatment of various diseases. However, its practical administration has been limited due to its poor aqueous solubility and bioavailability. It is found in the seeds of *Nigella sativa* (black seed), an annual flowering plant native to west-middle Asia and Mediterranean countries. While the seeds are used as a spice, the oil obtained from the seeds has been used traditionally in Arab culture for the treatment of arthritis, lung disease, and hypercholesterolemia. Studies have shown that the biological activity of the black seed is mainly from its essential oil components, especially the dominant (30–48%) thymoquinone [22]. The therapeutic effect of thymoquinone on cancer and inflammation has been demonstrated [22]. Thymoquinone has been found to be an effective free radical and superoxide radical scavenger, and it preserves the activity of various antioxidant enzymes such as catalase, glutathione peroxidase, and glutathione-S-transferase. This antioxidant effect is beneficial for many disease models, including experimental allergic encephalomyelitis, diabetes, asthma, and carcinogenesis in animals. It has been reported to exhibit anti-cancer effects through many mechanisms of action, including anti-proliferation, cell cycle arrest, stimulation of apoptosis, synergy with conventional medicine, generation of ROS (reactive oxygen species), and suppression of cancer metastasis and angiogenesis [22]. In addition, thymoquinone can reduce toxicity when used with conventional medical treatments. Various molecular targets for thymoquinone have been identified using cancer cell lines [23, 24].

In the present study, we explored the feasibility of developing a novel formulation of thymoquinone to treat and/or diagnose lung cancer. Thymoquinone was glucuronidated enzymatically and then conjugated with magnetic nanoparticles. The incorporation of these surface-modified nanoparticles into the matrix of carrier nanoparticles was successfully

Author Manuscript Author Manuscript Author Manuscript Author Manuscript

achieved. The anticancer effect and potential on tumor imaging of the engineered iron oxide nanoparticles were investigated *in vivo*.

## 2. MATERIALS AND METHODS

### 2.1. Materials

$Na^{131}I$ was provided by Şifa Hospital, Department of Nuclear Medicine. Iodogen (1,3,4,6-tetrachloro-3α,6 α-diphenylglycouril), ferrous chloride ($FeCl_3$) and ferric chloride tetrahydrate ($FeCl_2.4H_2O$) were purchased from Sigma-Aldrich. All other chemicals and cell culture reagents were purchased from Merck (New Jersey, USA), Sigma-Aldrich (Missouri, USA), Lonza (New Jersey, USA), Biowest (Texas, USA), and Promega (Wisconsin, USA). All solvents were reagent grade and used without further purification.

New Zealand male white rabbits weighing 4000–4500 g were used in MRI and SPECT studies, while 6–8-week old nude mice were used in *in vivo* tumor modeling studies. Both New Zealand white rabbits and Nu/Nu mice were purchased from Kobay A.S. (Ankara, Turkey).

### 2.2. Preparation of Thymoquinone Glucuronide (TQG) Conjugated Magnetic Iron Oxide Nanoparticles (TQGMNP)

Thymoquinone glucuronide (TQG) conjugated magnetic iron oxide nanoparticles (TQGMNP) were synthesized as previously described [6, 11, 25]. Briefly, the synthesis was completed in nine steps: 1) microsomal preparations from human lung carcinoma (A549) cells, 2) purification of UDP-glucuronyl transferase enzyme (UDPGT), 3) estimation of protein quantity in microsomal samples, 4) enzymatic glucuronidation reaction, 5) synthesis of magnetic ($Fe_3O_4$) nanoparticles, 6) preparation of magnetic nanoparticle conjugated TQG, 7) coating of $Fe_3O_4$ nanoparticles with silica, 8) amino silane conjugation of silica coated $Fe_3O_4$ nanoparticles, and 9) immobilization of TQG to amino silane conjugated $Fe_3O_4$ nanoparticles (TQGMNP).

**2.2.1. Microsomal Preparations from UDP-glucuronyl Transferases Enzyme (UDPGT) from A549 Cells—**Microsomal preparations extracted from A549 human lung carcinoma cells were used as a UDP-glucuronyl transferase (UDPGT) source, which was necessary for the enzymatic synthesis of thymoquinone glucuronide. In this step, A549 cells were grown in MEM supplemented with 10% fetal bovine serum (FBS), 2.0 mM glutamine, 0.1 mM nonessential amino acid, 1.5 g/L sodium bicarbonate, and 1 mM sodium pyruvate. The media were removed, and the cells were washed 3 times with PBS. The cells were detached from the surface and cell pellets were washed with sucrose/Hepes 3 times with centrifugation (4 °C, 1000 rpm and 10 min) in every step. Then, the cells were ruptured with a homogenizer for 4 minutes in an ice bath. The homogenate was centrifuged at 4 °C, 10500 rpm, for 10 min, and the supernatant was centrifuged at 4 °C, 28000 rpm, for 10 min using an ultracentrifuge. After centrifugation, the supernatant was removed, and then the enzymes were solubilized with a pH 7 buffer (0.2 M potassium phosphate, 2 mM mercaptoethanol and 0,4% Triton X100) and stirred at 4 °C for 30 min. Solubilized enzymes were centrifuged at 4 °C, 28000 rpm, for 10 min. The protein concentration of the supernatant containing the

Author Manuscript Author Manuscript Author Manuscript Author Manuscript

microsomal samples was determined by using the bicinchoninic acid method with a Thermo Fisher Varioskan Flash multimode microplate reader (Waltham, MA USA). Absorbance reading was performed at 260 nm; the obtained protein concentration was 3.44 mg/mL.

**2.2.2. Enzymatic Synthesis of Thymoquinone Glucuronide (TQG)—**34.4 mg microsomal preparation in 5 mL of 50 mM tris buffer (pH = 8), which contained 6 mM $CaCl_2$, 10 mM UDPGA, and 1 mM DTT was stirred at 37 °C for 10 min in a water bath. Then, thymoquinone in 10 mg/mL of DMSO was added and incubated at the same temperature for 18 h. After incubation, acetonitrile (300 μL) was added to the solution and centrifuged at 2000 rpm for 20 min. Purity analysis of the product was conducted by HPLC (Shimadzu LC10 ATVP).

### 2.2.3. Preparation of Magnetic Nanoparticles Conjugated with Thymoquinone (TQ) or TQG

**2.2.3.1. Synthesis of Magnetic Nanoparticles (Fe3O4):** One hundred mL of ferrous salt solution was prepared using 2 M $FeCl_3$ (12 mL) in 2 M HCl. Then, 0.08 M $Na_2SO_3$ (50 mL) was added slowly under nitrogen gas. $NH_3$ (25%, 8 mL) was added to the mixture under nitrogen gas. The mixture was left at 70 °C for 15–30 minutes. Then, the temperature was cooled to under 45° C. Black colored nanoparticles were collected with a magnet and washed with ethanol three times. Particles were stored at 4° C in ethanol.

**2.2.3.2. Silica Coating $Fe_3O_4$ Nanoparticles:** Five mL tetra ethyl ortho silicate (TEOS) and $NH_3$ (10%, 5 mL) was added into the magnetic particle solution. The reaction was carried out at 40 °C for 12 h under magnetic stirring. Then, it was washed with methanol 3 times.

**2.2.3.3. Amino Silane Conjugation of Silica Coated $Fe_3O_4$ Nanoparticles:** Amino silating agent [N-(2-Aminoethyl)-3-amino-propyltrimethoxysilane] was added into the magnetic nanoparticles in ethanol and the solution was kept in an ultrasonic bath for 5 min. After uniform dispersing, the reaction was carried out at 60 °C for 12 min and then washed with ethanol 3 times. The resulting precipitates were collected, dried under vacuum, and stored at 4° C.

**2.2.3.4. Immobilization of TQ and TQG to MNP Nanoparticles (TQMNP and TQGMNP):** Twenty-five mg/mL of silane modified MNP nanoparticles was washed with 0.1 M PBS, pH 7, at 25 °C. Then, nanoparticles were incubated with glutaraldehyde (2.5%) at 4°C in the ultrasonic bath for 4 hours. The suspension was centrifuged and washed with 0.1 M PBS. TQ (4 mg) and TQG (4 mg) were dissolved in 1 mL 0.1 M PBS which contained 0.15 M NaCl and 0.005 M EDTA (pH=7.2). After 12 h of incubation, particles were washed with 0.1 M borate tampon, which contained (pH=9.2) 0.5 mg/mL $NaBH_4$, and the particles were kept at 4°C for 30 min. The particles were then washed with 0.1 M PBS (pH=7.0 25°C) and resuspended in 1 mL 0.5 M MES (pH=6.6).

Author Manuscript Author Manuscript Author Manuscript Author Manuscript

### 2.3. High Performance Liquid Chromatography (HPLC) Analyses

TQ and enzymatically glucuronidated TQG were analyzed with HPLC (Shimadzu SCL-10AVP). A low pressure gradient HPLC system (LC-10ATvp quaternary pump, SPD-M20A DAD detector, a syringe injector equipped with a 500 1L loop, CTO-10AS column oven, SIL 20A-HT auto sampler, FRC-10A fraction collector, and 5μ C18-ODS column (250×4.6 mm ID)) was used for HPLC analysis. The mobile phase of analysis was water/methanol/isopropanol (50:45:5). The flow rate of the mobile phase was 1 mL/min and readings were collected at 254 nm.

### 2.4. Radiolabeling with $^{131}$I

Iodogen-coated tubes were prepared as containing 250 μg of iodogen. The solvent was allowed to evaporate, forming a thin solid layer on the wall of the reaction vial. Tubes were kept at 4 °C. 50 μg of samples was added to the iodogen-coated tubes and then 37 MBq/100 μL (1 mCi/0.1mL) Na$^{131}$I was added. The mixture was incubated for 30 min.

Then, thin layer radio chromatography (TLRC) was used to determine the radiolabeling yields. The developing bath consisted of n-butanol / bidistiled water / acetic acid (4:2:1). Two μL of radiolabeled ligand was applied to TLRC strips, which were then placed in the developing bath. After the mobile phase reached the endpoint, the TLRC strips were removed from the developing bath and left to dry. Bioscan AR2000 was used to obtain TLRC chromatograms. $R_f$ values of radiolabeled compounds and radiolabeling yields were calculated. $R_f$ values were found to be 0.39, 0.87, 0.45, 0.15, and 0.57 for $^{131}I^-$, $^{131}$I-TQ, $^{131}$I-TQG, $^{131}$I-TQMNP, and $^{131}$I-TQGMNP, respectively. The radiolabeling yields of all components were over 95%.

The iodogen method was also used for labeling with $^{127}$I for the structural analyses of iodinated TQ and TQG.

### 2.5. Inhaler Preparation

To prepare TQGMNP in inhaler form, TQGMNP and inhalation grade lactose (Lactohale 200) were mixed in a ratio of 1:100 (w/w) *via* geometric dilution to obtain a 1% binary blend. The formulation was blended uniformly in a glass mortar. After sufficient mixing, the formulation was passed through a sieve (60 mesh) and samples were stored in a desiccator at least 5 days prior to use.

### 2.6. Characterization of MNP Nanoparticles

The hydrodynamic diameters and the zeta potential of the synthesized nanoparticles and conjugates were measured with dynamic light scattering (DLS) using a Malvern Zetasizer Nano ZS (Malvern Panalytical, Malvern, UK) which measures the particle size distribution as well as the electrophoretic mobility of the dispersed particles. The measurement was repeated three times and the results were expressed as mean standard deviations.

Scanning electron microscope (SEM) and high-resolution transmission electron microscopy (HRTEM) images were obtained to determine the morphology of the nanoparticles.

Author Manuscript Author Manuscript Author Manuscript Author Manuscript

Fourier-transform infrared spectroscopy (FTIR) spectra were obtained with a Shimadzu IRTracer-10, (Kyoto, Japan) MIRacle ATR spectrometer (Attenuated Total Reflection).

### 2.7. Short-term Stability Test at Room Temperature

Three samples were prepared between low (25 μg/ml) to high (1000 μg/ml) concentrations. Samples were stored at room temperature (21–25°C) for up to 24 h and analyzed using HPLC at several time intervals (0, 2, 4, 6 and 24 h) under working conditions. Mean, standard deviation, and % relative standard deviation values of prepared concentrations were calculated.

### 2.8. Lipophilicity

For lipophilicity determination, the method by Zhang *et al.* was applied [26]. For this purpose, 0.3 mL of n-octanol and 0.3 mL of a pH 7 buffer were placed in a centrifuge tube, 0.1 mL of radiolabeled sample was added, and then the whole mixture was vortexed for 1 min. After being vortexed, the mixture was centrifuged at 2500 rpm for 30 min to form the upper (octanol) and the lower phase (water). 0.1 mL samples were taken from these phases, then they were counted using a Cd (Te) radioactivity detector. The procedure was repeated 5 times and logP values were calculated using the n-octanol to water ratios. The results were compared with the theoretical values obtained with the ACD program.

### 2.9. Preparation of Luciferase Transfected A549 (Luc-A549) Human Lung Carcinoma Cells

The firefly luciferase transfected A549 (Luc-A549) cell line was used in carcinogenesis studies described below. Luc-A549 cells were cultured in RPMI-1640 medium supplemented with 2 mM glutamine, 1.5 g/L sodium bicarbonate, 0.1 mM non-essential amino acids, 1 mM sodium pyruvate, and 10% FBS. All cells were grown at 37 °C in a humidified incubator equilibrated with 5% $CO_2$. The cells were maintained in exponential growth by subculturing with trypsin-EDTA. The cells were then pelleted and resuspended in the cell medium.

### 2.10. Ethics Approval and Consent To Participate

This study was approved by the ethics committee of Ege University Animal Ethics Committee, Izmir Turkey (2014-021) and Celal Bayar University Animal Ethics Committee, Manisa Turkey (2013-58).

**2.10.1. Human and Animal Rights—**No humans were involved in this study. All animal research procedures followed were in accordance with the standards of Guide for the US National Research Council's and Guide for the Care and Use of Laboratory Animals.

### 2.11. Modeling Lung Cancer *In Vivo*

To assess the antitumor effect of TQGMNP in a xenograft model, human lung cancer expressing luciferase (A549-Luc) was implanted subcutaneously ($5\times10^6$ cell) into Nu/Nu mice. TQGMNP was administered intravenously and in inhaler form. The IVIS imaging system was used to determine the changes in tumor volume by using bioluminescence light with a CCD camera. Further details are presented below.

Author Manuscript Author Manuscript Author Manuscript Author Manuscript

**2.11.1. Xenograft Tumor Model—**Twelve Nu/Nu mice at 6–7 weeks of age were kept under standard conditions (12 h light/dark) with food and water available. All twelve Nu/Nu mice were anesthetized with sevoflurane (2–4% / 100% $O_2$). Subcutaneous administration of $5\times10^6$ of cells in 100 μL PBS to the left or right half of the ventral cavity was accomplished. All tumors were allowed to grow for 2 weeks and mice were then used to perform *in vivo* imaging studies.

**2.11.2. Bioluminescence Imaging and In Vivo Anti-tumor Activity—**The tumor prevention study on tumor-bearing mice was initiated at day 7 after the implantation of Luc-A549 cells. Tumor-bearing mice were randomized into two groups (n=6 for each group): 1) the treated group, in which TQGMNP was injected intravenously in *isotonic sodium chloride solution* and 2) non-treated control group. Each animal was administered 100 μL of 12 mg luciferin/mL in pH 7 phosphate buffer solution (injected through the tail vein). In the treated group, 12 mg/kg TQGMNP was then administered. Bioluminescence images of animals were acquired with an optical imaging system (IVIS Spectrum, PerkinElmer, Massachusetts, USA) at days 1, 10 and 15. Circular regions of interest (ROI) were drawn for each tumor area for all animals and regional activities were quantified.

## 2.12. Full Body Distribution Evaluation Using MRI

Two healthy rabbits underwent MRI scanning on a 1.5 Tesla clinical scanner (Toshiba Exelart, Tokyo, Japan) to determine the full body distribution of TQGMNP. The rabbits were anesthetized with an intramuscular injection of ketamine/xylazine (10/40 mg/kg) cocktail and then were placed inside a quadrature coil with an 11 cm diameter circular surface coil. During MRI, the rabbits were intubated while they were maintained on anesthesia. MRI of the healthy rabbits was performed before and after 2 mg of TQGMNP in lactose powder inhaler form was administered. The biodistribution of TQGMNP was evaluated.

MRI consisted of a gradient echo imaging sequence with a flip angle of 20°, a repetition time of 2 s, a field of view of 13 cm, and echo times of 8.2, 40, 100, and 200 ms. Approximately 32 transaxial images were obtained with an in-plane resolution of 500 μm and a thickness of 1 mm.

The images were analyzed with an OsiriX DICOM viewer (Geneva, Switzerland). For each image, the organs of interest were manually segmented to quantify the total average signal intensity. The noise of the images was computed as the standard deviation of the mean signal of a region of interest (ROI) in the image background and the SNR was computed. The signal drop in each image was computed as the difference between the SNR in the lungs before (*i.e.*, baseline) and after TQGMNP administration, normalized to the SNR of the baseline images. All the ROIs in the lungs (right upper, left upper, right lower, and left lower lung zones) and in the liver were drawn while avoiding the main visible vessels.

## 2.13. Scintigraphic Studies

Three rabbits were anesthetized with intramuscular injections of ketamine/xylazine (10/40 mg/kg). The rabbits were placed in the prone position with their hind legs extended and

Author Manuscript Author Manuscript Author Manuscript Author Manuscript

ear vein access with a catheter was established. Thirty--seven MBq $^{131}$I-TQGMNP was intravenously injected into rabbits *via* the ear vein.

Both dynamic and static images were performed using a dual-headed gamma camera (Infinia, GE, Tirat Hacermel, Israel) equipped with high energy all-purpose parallel-hole collimators. Dynamic images were obtained over the first half hour with frames of 1 min after $^{131}$I-TQGMNP administration. Static images were also acquired after $^{131}$I- TQGMNP administration at 30, 90, 150, 210 min, and at 24 h in a 256×256 matrix using a zoom factor of 1.85 and a duration of 10 min. ROIs were drawn around the right lung, left lung, right kidney, left kidney, bowel, and liver. The right legs of the rabbits were regarded as suitable for drawing the background ROI and normalization against this region was performed. 100 mL blood samples were collected from the rabbits at 30, 90, 150, 210 min, and at 24 h. Blood samples were taken at certain time intervals, then counted on Cd (Te) detector and blood kinetics of $^{131}$I-TQGMNP were created by using these counts.

When the imaging procedure was completed, rabbits recovered in a housing unit and were monitored until awake.

### 2.14. Statistical Analysis

Student's t-test (unpaired and two-sided) was used to calculate P values. $P<0.05$ was considered significant for all analyses. All values were represented as means with standard deviations.

## 3. RESULTS

### 3.1. Characterization of Magnetic Nanoparticles

The structural properties of MNPs agree with our previous reports [11, 14]. The FTIR spectra (Fig. 1) showed peaks at around 3369 $cm^{-1}$ from the O—H stretching band and 550 $cm^{-1}$ from the Fe—O stretching band of magnetic nanoparticles. The peaks at 794 $cm^{-1}$ and 570 $cm^{-1}$ had symmetrical stress from the Si—O and Fe—O bands. In addition, the Si-O-Si asymmetric stretching band was detected at 1068 $cm^{-1}$, the Si-O symmetrical stress band at 790 $cm^{-1}$ and the Fe-O band at 571 $cm^{-1}$.

The FTIR peaks confirmed TQ glucuronidation in the spectrum. When the FTIR spectra of TQG glucuronide were examined, widespread OH peak intensity increased. Furthermore, while the C = O peak in thymoquinone (1688,02 $cm^{-1}$) was observed to decrease remarkably in the TQG molecule (1689,19 $cm^{-1}$), on the other hand, the C-O-C-asymmetric stretch of glucuronide bond that confirms glucuronidation was found around 1000 $cm^{-1}$.

$^{1}$H NMR chemical shift data (ppm) were used to confirm the structure of the TQ and TQG. $^{1}$H NMR (D6-DMSO): δ (ppm) 1.15 (aliphatic-CH3); 2.03 (aromatic–$CH_3$,), 3.17 (−$CH_2$), 6.38-6.63 (aromatic-CH) for TQ (Fig. 2). $^{1}$H NMR (D6-DMSO): δ (ppm) 1.15 (aliphatic-CH3); 1,10-2.10 (aromatic–$CH_3$,), 3.17 (−$CH_2$), 6.6-6.7 (aromatic-CH), 3.2-3.8 CH and 4.89 (OH) for TQG molecule (Fig. 3). The structures were also confirmed by the theoretical NMR data using the ACD/CHEMSKETCH software program.

Author Manuscript Author Manuscript Author Manuscript Author Manuscript

According to SEM images, the nanoparticles were very homogeneous and had a smooth surface and dimensions of 68,87±1,13 nm (Fig. 4A). The morphology and dimensions of coreshell nanoparticles were further determined using TEM (Fig. 4B, 4C), which showed that the dimensions of nanoparticles were 7,35±0,37 nm and they had rather polyhedral shapes. While the nanoparticle diameters obtained using TEM were comparable to those using SEM, the shape and size were better appreciated in TEM due to better solubility in TEM. In TEM images, the magnetic core was visible as a dark spot inside the bright spherical Si atoms. Our results agree with the data presented in our previous reports [6, 14].

The hydrodynamic diameters of the nanoparticles were 142,6±25,39t nm.

The shape and surface morphology of the particles in TQGMNP, TQGMNP-DPI and lactose formulations were studied using light microscopy at 40× magnification (Fig. 5). The images of both blank (Lactohale200) and MNP-loaded DPI formulations showed that the particles were not uniformly distributed, but smaller and smooth shaped particles were observed as expected (Table 1). Despite the methodological restrictions due to light microscopy technique, TQGMNP loaded onto lactose aggregates were seen clearly (Fig. 5).

### 3.2. MRI

Fig. (6) displays axial T2* MRI images with ROIs before and after administration of inhaler preparations of TQGMNP (TQGMNP loaded lactose).

Fig. (7) shows the maximum signal drop measured after the administration of TQGMNP loaded lactose and data are shown as the mean ± SD before and after treatment and normalized to the background. Overall, the change in the signal drop before and after treatment was significant, indicating the presence of iron particle accumulation in the lungs as well as in the liver. Within the lower lung zones, the signal drop was significantly higher.

### 3.3. Scintigraphic Studies

Lung uptake of $^{131}$I-labeled TQGMNP was observed at 30 min following administration (Fig. 8). As time progressed, the radioactivity in the liver increased as expected, due to the metabolic clearance of iron oxide nanoparticles. The highest lung-to-liver activity ratio was observed at 30 min post-injection, while at later timepoints (210 min and 24 h), most of the lung activity was cleared (Fig. 8). The negligible activity was found in major organs compared with the abdominal region after 24 h of injection (Fig. 8, 9, Table 2).

Blood activity was also calculated in parallel with scintigraphy imaging. Similar to the observations from the scintigraphy images, activity in the blood pool peaked at 30 min post-injection and rapid clearance was observed at 210 min post-injection (Fig. 10). The half-life of $^{131}$I-TQGMNP in the blood pool and the drug elimination rate was obtained from the slope of linear plots (activity versus t with the exponential function transformed to logarithmic function) (presented in Fig. 10 and Table 2). The half-life was calculated as 7.20 h using the equation given below.

Author Manuscript Author Manuscript Author Manuscript Author Manuscript

$$A_t = Ae^{-\lambda t}$$

Where: $A_t$= activity in blood at time t

A= activity in blood before administration of the drug

### 3.4. Antitumor Activity of TQGMNP in Tumor Xenografts *in vivo*

The mean tumor volume reduction was more apparent in mice treated with *isotonic sodium chloride solution (Group I: control)* compared to mice that received TQGMNP intravenously (*Group II:* Treatment) (twice a week). As shown in Fig. (11), after the treatment of mice with TQGMNP, xenograft tumor models disappeared after 10 and 15 days, respectively. Non-treated animals showed no significant reduction in tumor volume as expected. Moreover, in both groups of mice that were treated with TQGMNP, general recovery was observed while mice in the untreated control group experienced deterioration in their physical conditions (mobility, food consumption, drowsiness, and skin color).

Table 2 shows the right lung/background and liver/background ratios in the areas of interest.

## 4. DISCUSSION

In this study, we aimed to develop a theranostic tool that combines thymoquinone (TQ) with glucuronide (G) for the imaging and treatment of lung cancer. We added magnetic nanoparticles (MNP) to enable magnetic hyperthermia and MRI, as well as $^{131}I$ to enable SPECT imaging and radionuclide therapy.

Thymoquinone is a promising phytochemical compound for investigating inflammatory markers. In the literature, thymoquinone was shown to increase the p21 expression in lung adenocarcinoma and the p21 in the growth arrest of cancer cells. p21 expression has been demonstrated as an independent prognostic factor in patients with non-small cell lung carcinoma, and it may represent an important clinical marker of outcome in non-small cell lung carcinoma [22]. Thymoquinone has a phytochemical effect, as seen in the literature, but there has been no study on its imaging properties to date. This study was aimed at the inception of imaging studies of TQGMNP.

We combined thymoquinone with glucuronide, as some types of cancer, including lung cancer, are known to be rich in glucuronidase enzyme [18, 19, 27, 28]. This can be exploited in enzymatically directed drug targeting. Therefore, glucuronide derivatives of pharmacologically active compounds can act as prodrugs. The active compound is released at the desired site of action by endogenous glucuronidase enzymes [29]. Thymoquinone exists in tautomeric forms, including the enol form, the keto form and mixtures (30). Although the keto form is the main fraction (~ 90%), the glucuronidation reaction proceeds through the enol form. Therefore, thymoquinone glucuronide has a phenol ring in its structure. As seen from the spectra obtained in our study, the C=O peak disappeared while the intensity of the OH peak increased.

Author Manuscript Author Manuscript Author Manuscript Author Manuscript

The anticancer effect of thymoquinone has been demonstrated in both *in vivo* and *in vitro* studies on several types of tumor cells, including lung cancer [30-36]. Thymoquinone's mechanisms of action in cancer, aside from radical scavenging, might also include anti-proliferation, cell cycle arrest, and apoptosis [32-36]. Attoub *et al.* reported the activity of thymoquinone against non-small cell lung cancer and small cell lung cancer cell lines alone and in combination with Cisplatin. In their study, thymoquinone was able to inhibit cell proliferation, reduce cell viability, and induce apoptosis. Thymoquinone at 100 μM inhibited cell proliferation by nearly 90% [32].

We added magnetic nanoparticles to TQG as magnetic nanoparticles are effective platforms for targeted therapy and for theranostics. They have been used to improve the therapeutic performance of drugs and reduce the side effects associated with the conventional treatment of cancer. Lübbe *et al.* first reported clinical experiments in human patients with magnetic drug targeting, showing that it was well tolerated [37]. In our study, the incorporation ratios of TQGMNP with A549 cells were seen at the highest levels. In both inhaler and intravenous applications, the lung targeting of TQGMNP indicates that these particles are very suitable for targeted radionuclide therapy. Previous studies have suggested that while smaller molecules are mainly excreted by the kidney, clearance of iron oxide nanoparticles occurs through the hepatic pathway [9, 37], which our results support. In addition to our findings in the current study, previously, we reported that TQGMNP was able to inhibit apoptosis on A549 cells; however, there was no apoptotic effect of the samples on BEAS-2B cells [6]. Size distribution, cellular uptake, and toxicity characteristics of TQGMNP make it a useful, targeted delivery system in lung cancer diagnosis and therapy [6].

Lastly, we labeled TQGMNP with $^{131}$I. $^{131}$I-labeled conjugates are preferred tracers for cell tracking. $^{131}$I has a physical half-life of 8 days and is used clinically as a beta emitting therapeutic radionuclide of iodine. As a theranostic radionuclide of iodine, its wide range of decay properties is well suited for therapy as well as imaging [38].

Matsumoto *et al.* reported that tumor development was completed within two weeks of lung cancer tumor models using A549 cells. In our experiments, tumor formation was completed within 15 days and results were consistent with the literature [39].

## CONCLUSION

$^{131}$I-TQGMNP has the potential for theranostic applications and imaging with MRI and SPECT. $^{131}$I-TQGMNP can also be used in *in vitro* cancer kits for the diagnosis of different cancers rich in the beta-glucuronidase enzyme. By virtue of the magnetic property imparted by the magnetic nanoparticles, hybrid therapy comprised of tumor-targeting drugs and magnetic hyperthermia can be used for different tumors. The information gathered from this work may be helpful for the design and synthesis of a novel multi-modal therapeutic agent to detect and treat lung cancer.

Author Manuscript Author Manuscript Author Manuscript Author Manuscript

## FUNDING

This project was financially supported by the Turkish Scientific Research Council- Health Sciences Research Support Group (TUBİTAK-SBAG; Project No: 113S922), Ankara, Turkey. Omer Aras was supported in part by the NIH/NCI Cancer Center Support Grant P30 CA008748.

## REFERENCES

[1]. Hirsch FR; Franklin WA; Gazdar AF; Bunn PA Jr, Early detection of lung cancer: clinical perspectives of recent advances in biology and radiology. Clin. Cancer Res, 2001, 7(1), 5–22. PMID: 11205917 [PubMed: 11205917]

[2]. Sohail MF; Rehman M; Sarwar HS; Naveed S; Salman O; Bukhari NI; Hussain I; Webster TJ; Shahnaz G Advancements in the oral delivery of Docetaxel: challenges, current state-of-the-art and future trends. Int. J. Nanomedicine, 2018, 13, 3145–3161. 10.2147/IJN.S164518 PMID: 29922053 [PubMed: 29922053]

[3]. Lin L; Wong H Predicting Oral Drug Absorption: Mini Review on Physiologically-Based Pharmacokinetic Models. Pharmaceutics, 2017, 9(4), 41. 10.3390/pharmaceutics9040041 PMID: 28954416

[4]. Li K; Nejadnik H; Daldrup-Link HE Next-generation superparamagnetic iron oxide nanoparticles for cancer theranostics. Drug Discov. Today, 2017, 22(9), 1421–1429. 10.1016/j.drudis.2017.04.008 PMID: 28454771 [PubMed: 28454771]

[5]. Häfeli UO; Sweeney SM; Beresford BA; Humm JL; Macklis RM Effective targeting of magnetic radioactive 90Y-microspheres to tumor cells by an externally applied magnetic field. Preliminary *in vitro* and *in vivo* results. Nucl. Med. Biol, 1995, 22(2), 147–155. 10.1016/0969-8051(94)00124-3 PMID: 7767307 [PubMed: 7767307]

[6]. Ince I; Müftüler ZB; Medine Eİ; Güldü KO; Tekin V; Aktar S; Göker E; Unak P Synthesis of Radioiodinated Thymoquinone Glucuronide Conjugated Magnetic Nanoparticle (125I-TQG-Fe3O4) and its Cytotoxicity and *in vitro* Affinity. Acta Pharm. Sci, 2018, 56(2), 7–26.

[7]. Briley-Saebo K; Bjørnerud A; Grant D; Ahlstrom H; Berg T; Kindberg GM Hepatic cellular distribution and degradation of iron oxide nanoparticles following single intravenous injection in rats: implications for magnetic resonance imaging. Cell Tissue Res., 2004, 316(3), 315–323. 10.1007/s00441-004-0884-8 PMID: 15103550 [PubMed: 15103550]

[8]. Longmire M; Choyke PL; Kobayashi H Clearance properties of nano-sized particles and molecules as imaging agents: considerations and caveats. Nanomedicine (Lond.), 2008, 3(5), 703–717. 10.2217/17435889.3.5.703 PMID: 18817471 [PubMed: 18817471]

[9]. Arami H; Khandhar A; Liggitt D; Krishnan KM *in vivo* delivery, pharmacokinetics, biodistribution and toxicity of iron oxide nanoparticles. Chem. Soc. Rev, 2015, 44(23), 8576–8607. 10.1039/C5CS00541H PMID: 26390044 [PubMed: 26390044]

[10]. Mirković M; Radović M; Stanković D; Milanović Z; Janković D; Matović M; Jeremić M; Antić B; Vranješ-Đurić S $^{99m}$Tc-bisphosphonate-coated magnetic nanoparticles as potential theranostic nanoagent. Mater. Sci. Eng. C, 2019, 102, 124–133. 10.1016/j.msec.2019.04.034 PMID: 31146983

[11]. Medine IE; Unak P; Sakarya S; Toksöz F Enzymatic synthesis of uracil glucuronide, labeling with 125/131**I**, and *in vitro* evaluation on adenocarcinoma cells. Cancer Biother. Radiopharm, 2010, 25(3), 335–344. 10.1089/cbr.2009.0727 PMID: 20578839 [PubMed: 20578839]

[12]. Bekis R; Biber Z; Dagdeviren K; Ertay T; Unak P Effect of I-131 labelled magnetic iron particles in breast tumor. Eur. J. Nucl. Med. Mol. Imaging, 2009, 36(S2), S400–S400.

[13]. Dagdeviren K; Unak P; Bekis R; Biber FZ; Akdurak S; Ulker O; Ergur B; Ertay T; Durak H Radioiodinated magnetic targeted carriers (I-131-MTC). J. Radioanal. Nucl. Chem, 2007, 273(3), 635–639. 10.1007/s10967-007-0923-5

[14]. Ozkaya F; Unak P; Medine EI; Sakarya S; Unak G; Timur S (18)FDG conjugated magnetic nanoparticle probes: synthesis and *in vitro* investigations on MCF-7 breast cancer cells. J. Radioanal. Nucl. Chem, 2013, 295(3), 1789–1796. 10.1007/s10967-012-2248-2

[15]. Shanehsazzadeh S; Gruettner C; Yousefnia H; Lahooti A; Gholami A; Nosrati S; Zolghadri S; Anijdan SHM; Lotfabadi A; Varnamkhasti BS Development of Lu-177-DTPA-SPIO conjugates

Author Manuscript Author Manuscript Author Manuscript Author Manuscript

for potential use as a dual contrast SPECT/MRI imaging agent. Radiochim. Acta, 2016, 104(5), 337–344. 10.1515/ract-2015-2499

[16]. Jordan CD; Han M; Kondapavulur S; Vera DB; Neumann KD; Moore T; Stillson C; Krug R; Behr S; Seo Y; Van-Brocklin HF; Larson PEZ; Wilson M; Martin AJ; Hetts SW Quantification of $^{89}$ Zr-Iron oxide nanoparticle biodistribution using PET-MR and ultrashort TE sequences. J. Magn. Reson. Imaging, 2018, 48(6), 1717–1720. 10.1002/jmri.26193 PMID: 29761624 [PubMed: 29761624]

[17]. Wu Y; Briley-Saebo K; Xie J; Zhang R; Wang Z; He C; Tang CY; Tao X Inflammatory bowel disease: MR- and SPECT/CT-based macrophage imaging for monitoring and evaluating disease activity in experimental mouse model--pilot study. Radiology, 2014, 271(2), 400–407. 10.1148/radiol.13122254 PMID: 24475849 [PubMed: 24475849]

[18]. Unak P Radionuclide Labeled Glucuronide Prodrugs for Imaging and Targeting Therapy of Cancer. Neuro-Oncology And Cancer Targeted Therapy; Gutierrez LM, Ed.; Cancer Etiology Diagnosis and Treatments, 2010, pp. 239–248.

[19]. Sperker B; Backman JT; Kroemer HK The role of beta-glucuronidase in drug disposition and drug targeting in humans. Clin. Pharmacokinet, 1997, 33(1), 18–31. 10.2165/00003088-199733010-00003 PMID: 9250421

[20]. Su YC; Cheng TC; Leu YL; Roffler SR; Wang JY; Chuang CH; Kao CH; Chen KC; Wang HE; Cheng TL PET imaging of β-glucuronidase activity by an activity-based 124I-trapping probe for the personalized glucuronide prodrug targeted therapy. Mol. Cancer Ther, 2014, 13(12), 2852–2863. 10.1158/1535-7163.MCT-14-0212 PMID: 25277385 [PubMed: 25277385]

[21]. Martin V Overview of paclitaxel (TAXOL). Semin. Oncol. Nurs, 1993, 9(4)(Suppl. 2), 2–5. 10.1016/S0749-2081(16)30035-3 PMID: 7904376

[22]. Woo CC; Kumar AP; Sethi G; Tan KHB Thymoquinone: potential cure for inflammatory disorders and cancer. Biochem. Pharmacol, 2012, 83(4), 443–451. 10.1016/j.bcp.2011.09.029 PMID: 22005518 [PubMed: 22005518]

[23]. Banerjee S; Padhye S; Azmi A; Wang Z; Philip PA; Kucuk O; Sarkar FH; Mohammad RM Review on molecular and therapeutic potential of thymoquinone in cancer. Nutr. Cancer, 2010, 62(7), 938–946. 10.1080/01635581.2010.509832 PMID: 20924969 [PubMed: 20924969]

[24]. Worthen DR; Ghosheh OA; Crooks PA The *in vitro* anti-tumor activity of some crude and purified components of blackseed, Nigella sativa L. Anticancer Res., 1998, 18(3A), 1527–1532. PMID: 9673365 [PubMed: 9673365]

[25]. Ediz M; Avcıbaşı U; Unak P; Muftuler FZB; Medine EI; Kılcar AY; Demiroglu H; Gumuser FG; Sakarya S Investigation Of Therapeutic Efficiency Of Bleomycin (BLM) And Bleomycin-Glucuronide (BLMG) Labeled With Radioactive (131)I On The Cancer Cell Lines. Cancer Biother. Radiopharm, 2013, 28(4), 310–319. 10.1089/cbr.2012.1316 PMID: 23350895 [PubMed: 23350895]

[26]. Zhang L; Li ZG; Huang RQ Wang QS Lipophilicity determination of N- (benzothiazol-2-yl) -α-amino alkyl phosphonic diesters by RP-HPLC and RP-HPTLC. Chin. J. Chem, 2000, 18(6), 872–876. 10.1002/cjoc.20000180614

[27]. Sperker B; Werner U; Mürdter TE; Tekkaya C; Fritz P; Wacke R; Adam U; Gerken M; Drewelow B; Kroemer HK Expression and function of beta-glucuronidase in pancreatic cancer: potential role in drug targeting. Naunyn Schmiedebergs Arch. Pharmacol, 2000, 362(2), 110–115. 10.1007/s002100000260 PMID: 10961372 [PubMed: 10961372]

[28]. Stevenson DE Optimization UDP-glucuronyl transferase-catalysed synthesis of testosteronβ-D-glucuronide by inhibition of contaminating β-glucuronidase. Biotechnol. Tech, 1999, 13, 17–21. 10.1023/A:1008857331429

[29]. Chen X; Wu B; Wang PG Glucuronides in anti-cancer therapy. Curr. Med. Chem. Anticancer Agents, 2003, 3(2), 139–150. 10.2174/1568011033353470 PMID: 12678908 [PubMed: 12678908]

[30]. Arroo RRJ; Alfa HH Chemical properties of thymoquinone, a monoterpene isolated from the seeds of Nigella sativa Linn. Pharmacol. Res, 2018, 133, 151. 10.1016/j.phrs.2018.05.003 PMID: 29777758 [PubMed: 29777758]

Author Manuscript Author Manuscript Author Manuscript Author Manuscript

[31]. Ulasli SS; Celik S; Gunay E; Ozdemir M; Hazman O; Ozyurek A; Koyuncu T; Unlu M Anticancer effects of thymoquinone, caffeic acid phenethyl ester and resveratrol on A549 non-small cell lung cancer cells exposed to benzo(a)pyrene. Asian Pac. J. Cancer Prev, 2013, 14(10), 6159–6164. 10.7314/APJCP.2013.14.10.6159 PMID: 24289642 [PubMed: 24289642]

[32]. Attoub S; Sperandio O; Raza H; Arafat K; Al-Salam S; Al Sultan MA; Al Safi M; Takahashi T; Adem A Thymoquinone as an anticancer agent: evidence from inhibition of cancer cells viability and invasion *in vitro* and tumor growth *in vivo*. Fundam. Clin. Pharmacol, 2013, 27(5), 557–569. 10.1111/j.1472-8206.2012.01056.x PMID: 22788741 [PubMed: 22788741]

[33]. Li F; Rajendran P; Sethi G Thymoquinone inhibits proliferation, induces apoptosis and chemosensitizes human multiple myeloma cells through suppression of signal transducer and activator of transcription 3 activation pathway. Br. J. Pharmacol, 2010, 161(3), 541–554. 10.1111/j.1476-5381.2010.00874.x PMID: 20880395 [PubMed: 20880395]

[34]. Nagi MN; Mansour MA Protective effect of thymoquinone against doxorubicin-induced cardiotoxicity in rats: a possible mechanism of protection. Pharmacol. Res, 2000, 41(3), 283–289. 10.1006/phrs.1999.0585 PMID: 10675279 [PubMed: 10675279]

[35]. Shoieb AM; Elgayyar M; Dudrick PS; Bell JL; Tithof PK *in vitro* inhibition of growth and induction of apoptosis in cancer cell lines by thymoquinone. Int. J. Oncol, 2003, 22(1), 107–113. 10.3892/ijo.22.1.107 PMID: 12469192 [PubMed: 12469192]

[36]. Al-Qubaisi MS; Rasedee A; Flaifel MH; Eid EEM; Hussein-Al-Ali S; Alhassan FH; Salih AM; Hussein MZ; Zainal Z; Sani D; Aljumaily AH; Saeed MI Characterization of thymoquinone/hydroxypropyl-β-cyclodextrin inclusion complex: Application to anti-allergy properties. Eur. J. Pharm. Sci, 2019, 133, 167–182. 10.1016/j.ejps.2019.03.015 PMID: 30902654 [PubMed: 30902654]

[37]. Lübbe AS; Alexiou C; Bergemann C Clinical applications of magnetic drug targeting. J. Surg. Res, 2001, 95(2), 200–206. 10.1006/jsre.2000.6030 PMID: 11162046 [PubMed: 11162046]

[38]. Unak P; Cetinkaya B Absorbed dose estimates at the cellular level for 131**I**. Appl. Radiat. Isot, 2005, 62(6), 861–869. 10.1016/j.apradiso.2004.07.013 PMID: 15799863 [PubMed: 15799863]

[39]. Matsumoto S; Tanaka F; Sato K; Kimura S; Maekawa T; Hasegawa S; Wada H Monitoring with a non-invasive bioluminescent *in vivo* imaging system of pleural metastasis of lung carcinoma. Lung Cancer, 2009, 66(1), 75–79. 10.1016/j.lungcan.2008.12.010 PMID: 19178977 [PubMed: 19178977]

Author Manuscript Author Manuscript Author Manuscript Author Manuscript

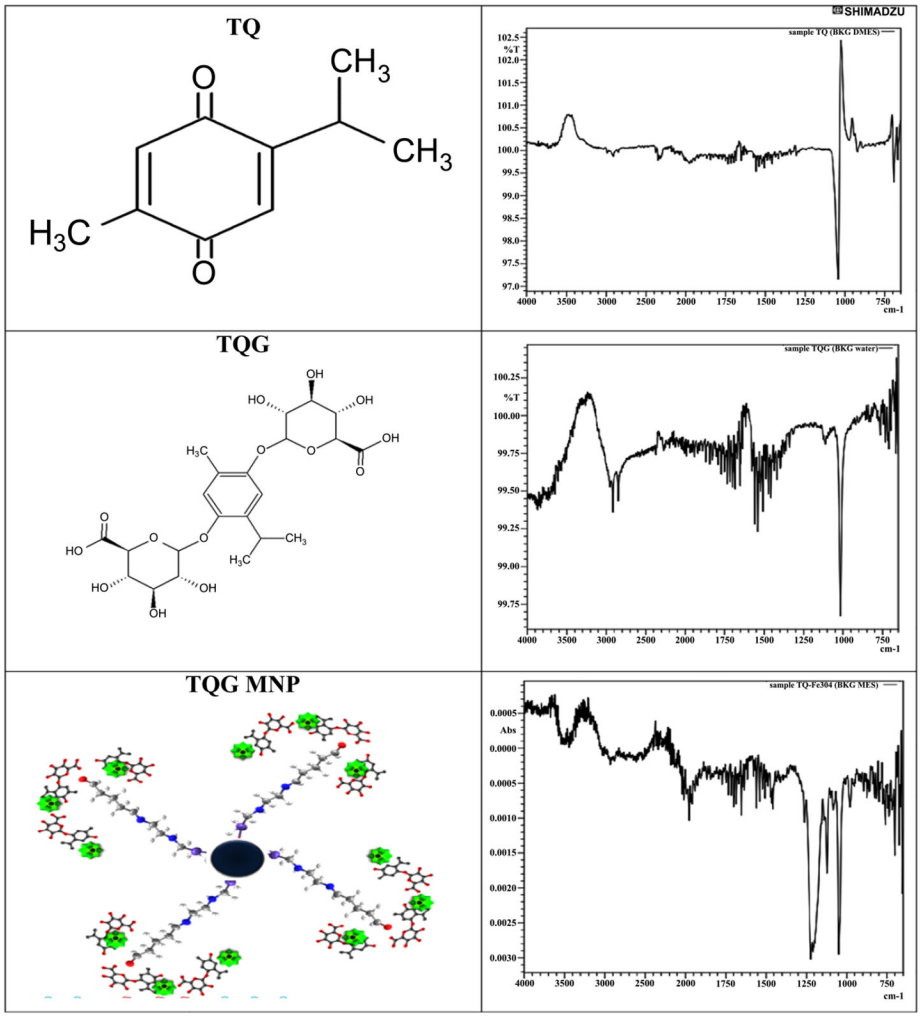



**Fig. (1).**
FTIR Spectra of Thymoquinone (TQ) and Thymoquinone glucuronide (TQG).

Author Manuscript Author Manuscript Author Manuscript Author Manuscript

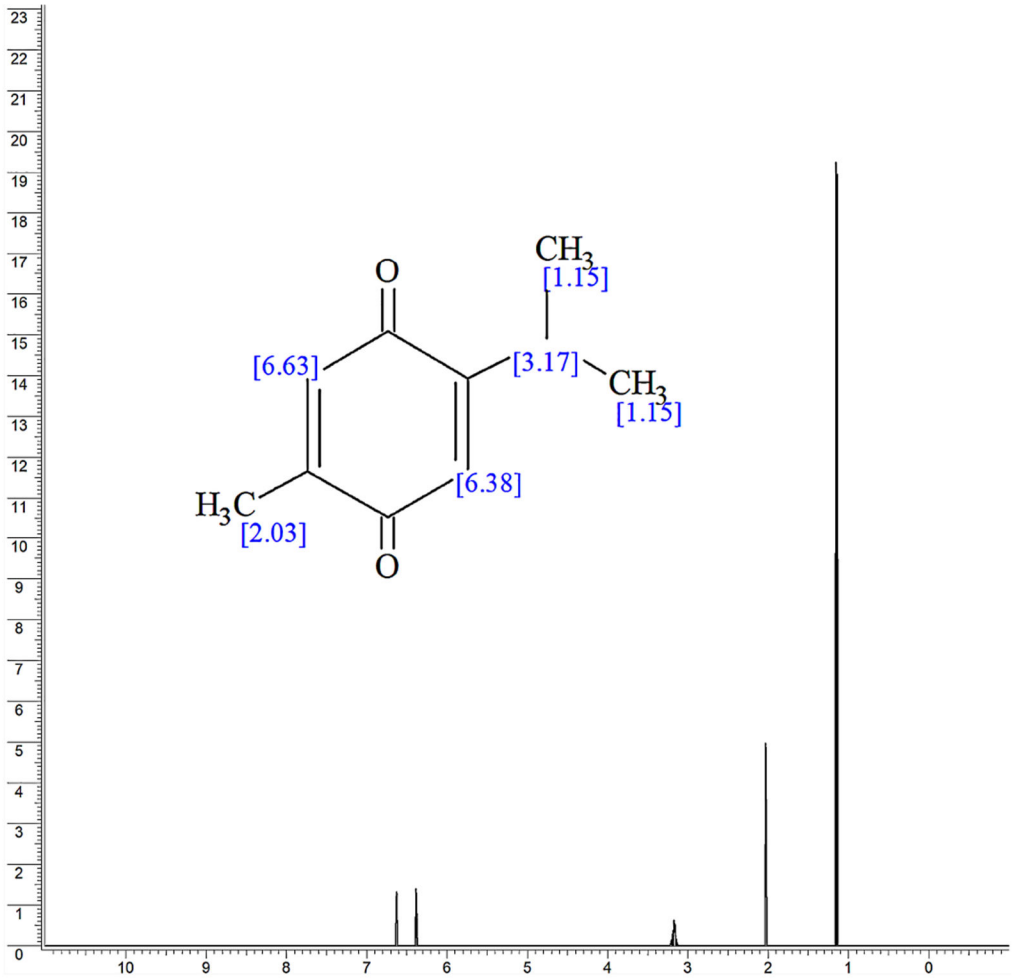



**Fig. (2).**
The $^{1}$H NMR Spectra of thymoquinone (TQ).

Author Manuscript Author Manuscript Author Manuscript Author Manuscript

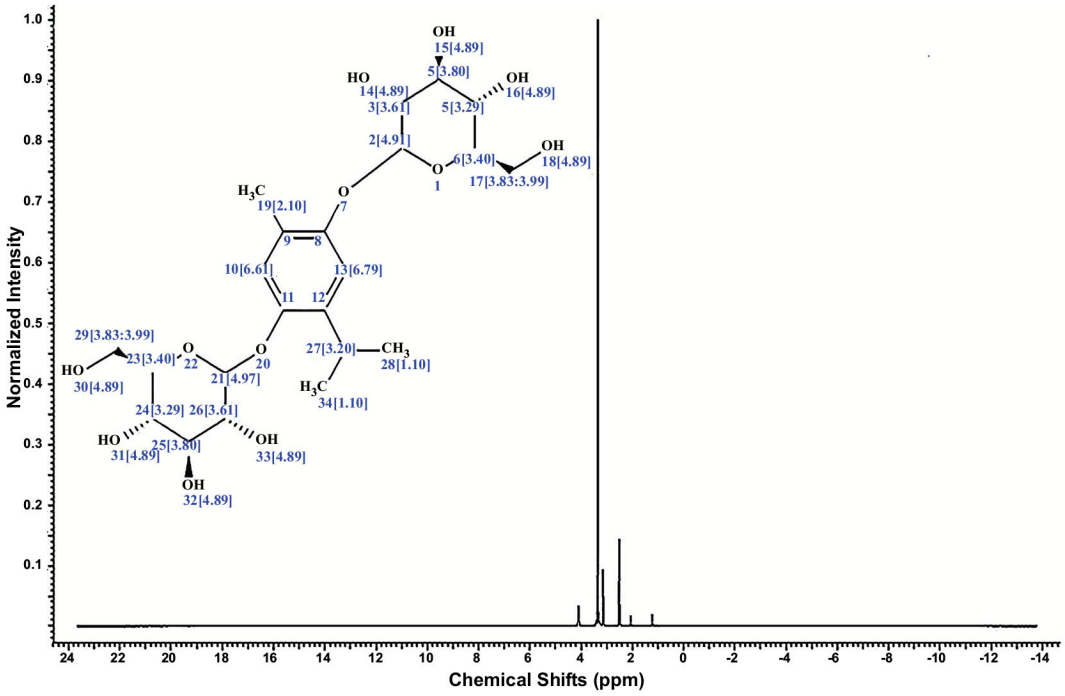



**Fig. (3).**
The $^{1}$H NMR Spectra of thymoquinone glucuronide (TQG).

Author Manuscript Author Manuscript Author Manuscript Author Manuscript

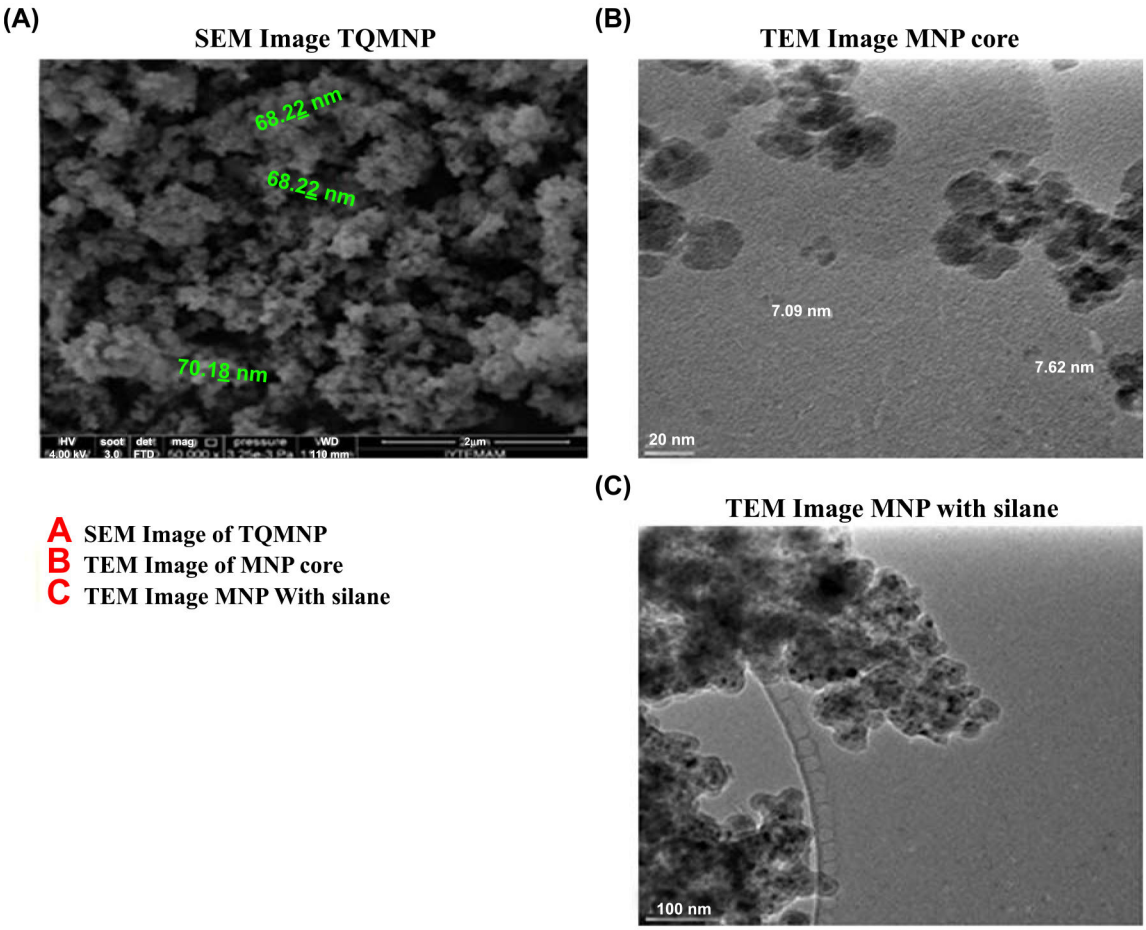



**Fig. (4).**
SEM versus TEM images.

Author Manuscript Author Manuscript Author Manuscript Author Manuscript

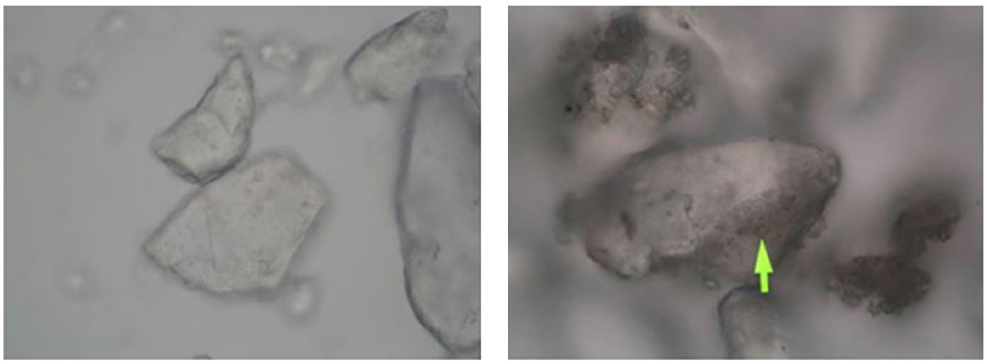


**Fig. (5).**
The images of both blank (Lactohale200) and MNP-loaded DPI formulations.

Author Manuscript Author Manuscript Author Manuscript Author Manuscript

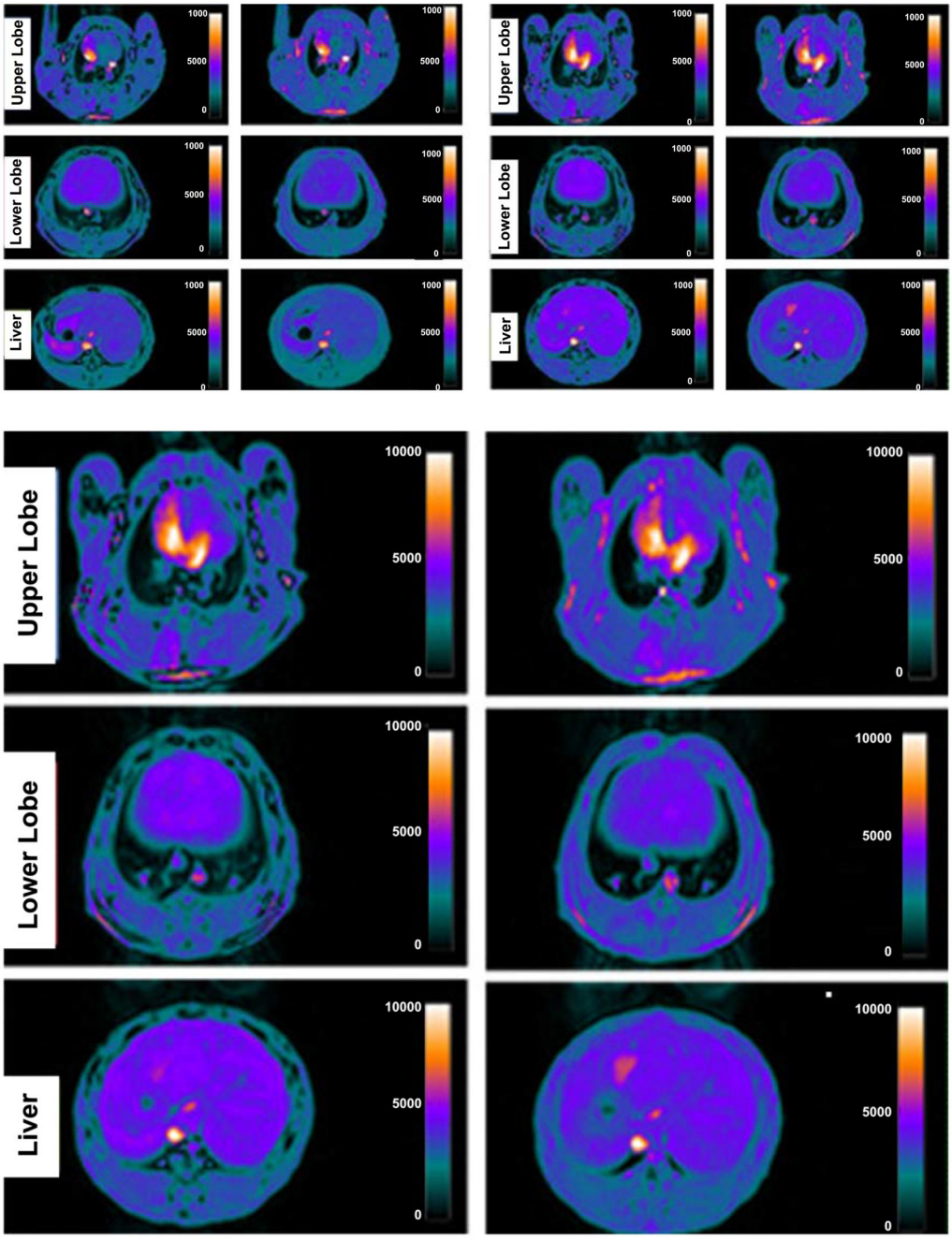



**Fig. (6).**
T2* MRI images with ROIs before and after administration of inhaler preparations of TQGMNP (TQGMNP loaded lactose).

Author Manuscript Author Manuscript Author Manuscript Author Manuscript

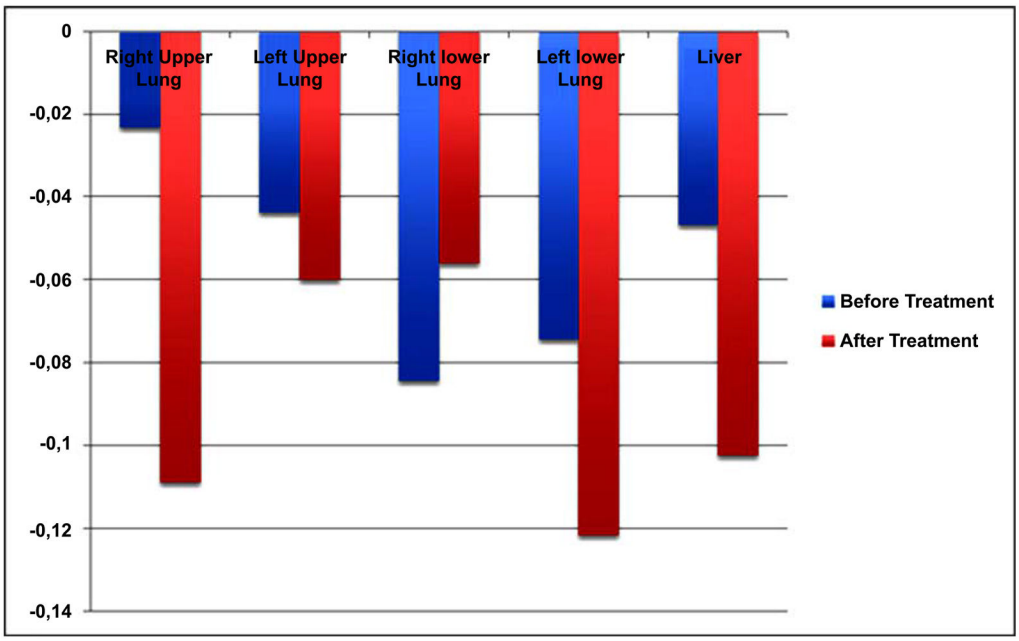



**Fig. (7).**
Bar plot shows the drop of signal intensities in bilateral upper and lower zones as well as in the liver before and after treatment.

Author Manuscript Author Manuscript Author Manuscript Author Manuscript

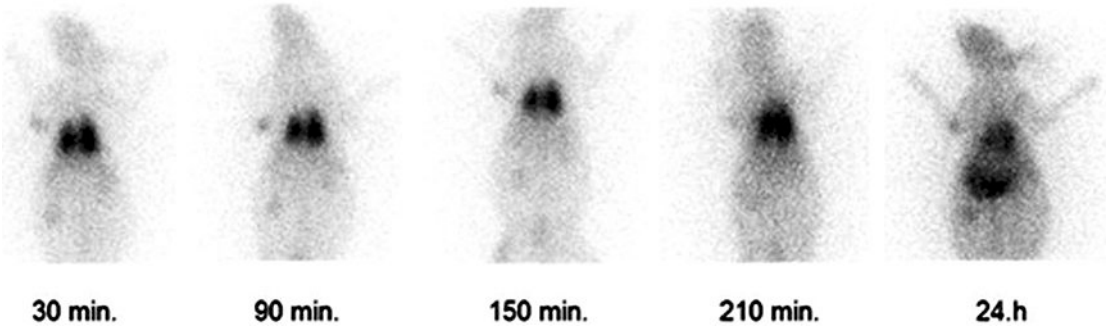



**Fig. (8).**
Scintigraphic images of the rabbits obtained at 30, 90, 150, 210 min, and at 24 h after 131**I**-TQGMNP administration.

Author Manuscript Author Manuscript Author Manuscript Author Manuscript

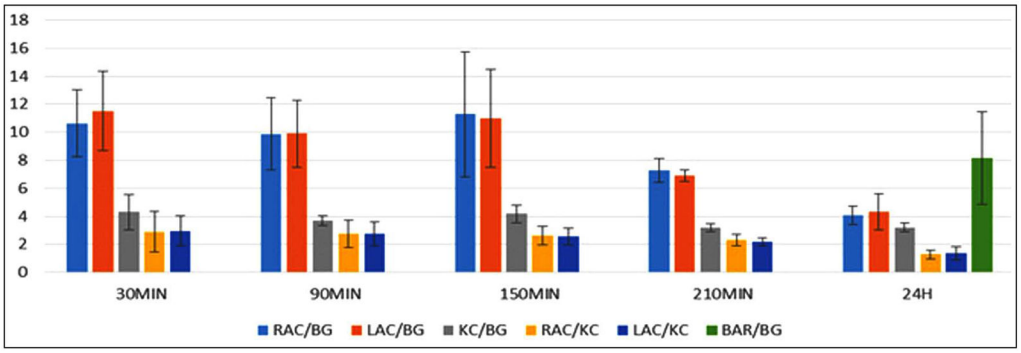



**Fig. (9).**

Right lung (RL)/background (BG), left lung (LL)/BG, liver (Liv)/BG, RL/Liv and LL/Liv. Ratios obtained at 30, 90, 150, 210 min, and at 24 h after 131**I**-TQGMNP administration; error bars represent the standard deviation.

Author Manuscript Author Manuscript Author Manuscript Author Manuscript

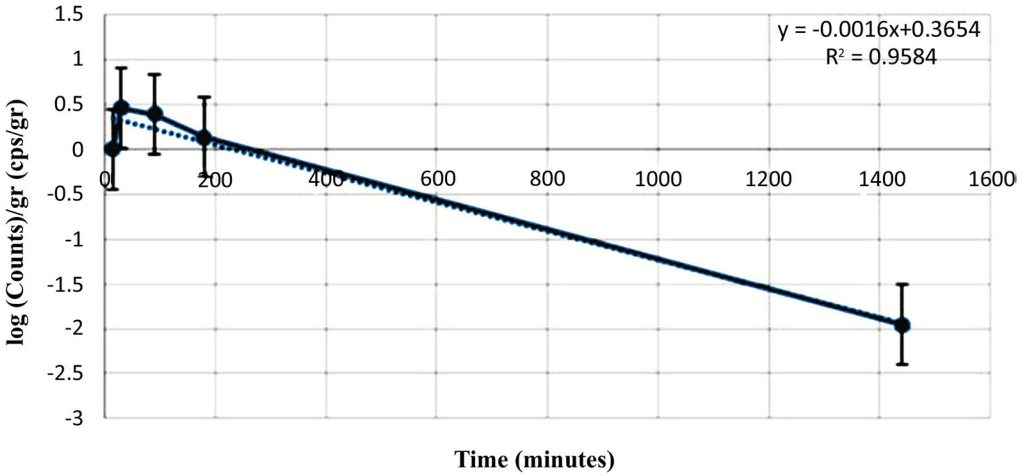



**Fig. (10).**

Decay of $^{131}$I radioactivity in the blood (log counts/gr) by time (min) after intravenous application of $^{131}$I-TQGMNP.

Author Manuscript Author Manuscript Author Manuscript Author Manuscript

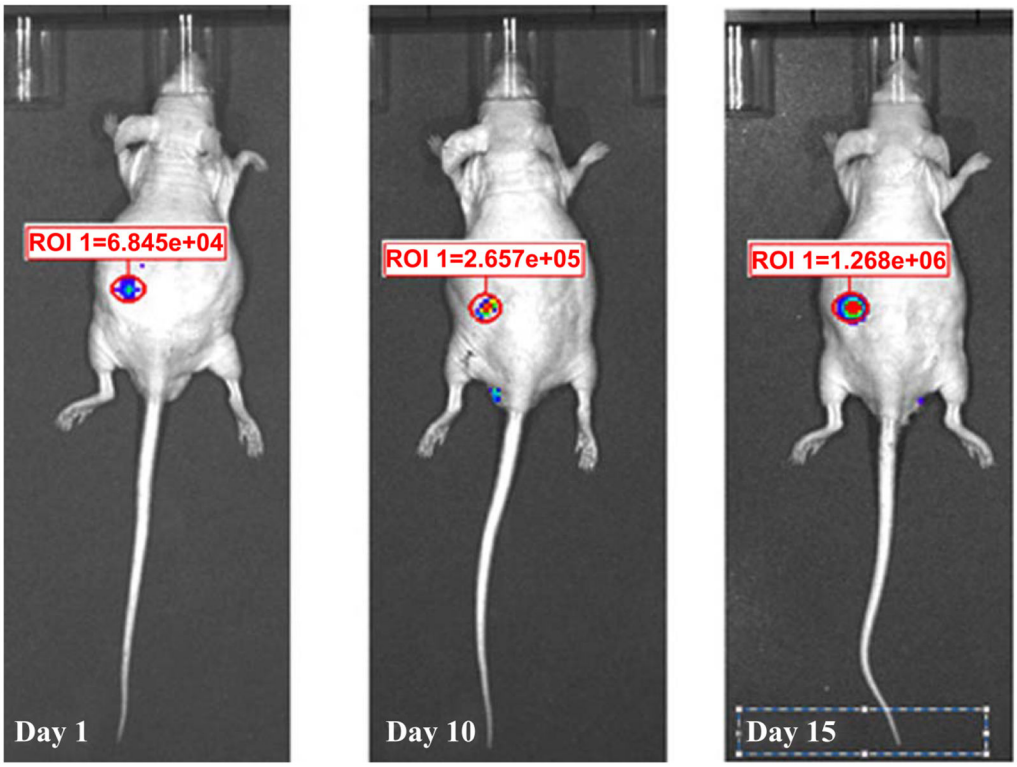



**Fig. (11).**
Time course of whole-mouse imaging with Xenogen IVIS 200 system after intravenous TQGMNP administration into Luc-A549-bearing mice.

Author Manuscript Author Manuscript Author Manuscript Author Manuscript

**Table 1.**

DPI particle size distribution.

| DPI Particle Size Distribution | Particle Size (μm) | | |
|---|---|---|---|
| | Lactose (Lactohale-200) | Lactose & TQGMNP DPI | TQGMNP |
| D(10) | 9 | 28.5 | 1,70 |
| D(50) | 74 | 84.2 | 3,90 |
| D(90) | 156 | 161 | 9.51 |

Author Manuscript Author Manuscript Author Manuscript Author Manuscript

**Table 2.**

RL/BG and Liv/BG ratios in the areas of interest.

| | 30 min | 90 min | 150 min | 210 min | 24 hour |
|---|---|---|---|---|---|
| RL/BG | 10.63 | 9.88 | 11.28 | 7.29 | 4.07 |
| LL/BG | 11.51 | 9.89 | 10.99 | 6.89 | 4.31 |
| Liv/BG | 4.30 | 3.70 | 4.163 | 3.20 | 3.21 |